
Bachelor Thesis

# Topological Hall Effect of $EuCd_2As_2$

Submitted by

**Rafael Spörri**

**Supervisors:**
**Dr. Yang Xu**
**Prof. Johan Chang**

June 2020

Laboratory for Quantum Matter Research
Physik Institut at University of Zürich

# *Abstract*

The interest of studying the anomalous Hall effect in exposure of magnetism and temperature lead to this study on the antiferromagnet $EuCd_2As_2$. It is a combined electrical and thermoelectrical transport study and should give us a better understanding of the topology as a new organizing principle of quantum matters. The data was obtained by using commercial Quantum Design Magnetic and Physical Property Measurement Systems (MPMS and PPMS).
In this work, we discuss the extraction of the topological Hall effect from measurements of the overall Hall effect of $EuCd_2As_2$. This is done with separating the overall Hall resistivity into the ordinary Hall effect and the anomalous Hall effect. The anomalous Hall effect is then further split into the contributions extraordinary Hall effect and topological Hall effect (THE). The theoretical working principles of Hall effects are discussed in the introductory section to reason the equations later used in the data processing. With the linear fitting method of Origin Lab the data is separated, leading to two final 3D colour plots showing the topological Hall resistivity in dependence of the applied magnetic field strength and temperature. The discussion of the source of both, the paramagnetic (PM) and antiferromagnetic (AFM) state, leads to Weyl points (momentum-space scenario) which is also in accordance with other studies. However the real-space scenario can't be excluded in the AFM state. The different behaviours of the THE isotherms in PM and AFM state seem to point to a vivid interplay of topology and magnetism in $EuCd_2As_2$ which may be a topic for future studies.

# *Zusammenfassung*

Das Interesse an Studien über den anonalous Hall-effekt in Kombination mit Magnetismus und Temperatur führte zu dieser Studie am Antferromagneten $EuCd_2As_2$. Es handelt sich um eine kombinierte elektrische und thermoelektrische Transport-Studie und sollte uns ein besseres Verständnis über die Topologie als neues Organisationsprinzip für Quantenmaterie geben. Die Daten wurden mit einem kommerziellen System zur Messung physikalischer Eigenschaften (PPMS) und mit einem System zur Messung magnetischer Eigenschaften (MPMS) gemessen.
In dieser Arbeit diskutieren wir die Extraktion des topologischen Hall-Effekts aus den gemessenen Daten des gesamten Hall-Effekts bei $EuCd_2As_2$. Dafür wird der gemessene Hall-Effekt in die Anteile des gewöhnlichen Hall-Effekts und des abnormalen Hall-Efekts geteilt. Letzterer kann weiter in einen aussergewöhnlichen Hall-Effekt und den gesuchten topologischen Hall-Effekt (THE) zersetzt werden. Die theoretischen Grundlagen der verschiedenen Effekte werden in der Einleitung besprochen um das spätere Einsetzten dieser Gleichungen in der Datenverarbeitung zu rechtfertigen. Das Endresultat kann in zwei 3D Farbplotts dargestellt werden, welche den spezifischen topologischen Hall-Wiederstand in Abhängigkeit des angelegten magnetischen Feldes und der Materialtemperatur zeigen. Die Diskussion des Plots, sowohl im antiferromagnetischen (AFM) als auch im paramagnetischen (PM) Bereich, führt uns zu Weyl Punkten (Szenario des reziproken Impuls-Raums) als Ursache, was auch in Übereinstimmung mit Resultaten anderer Studien ist. Allerdings kann ein Anteil vom realen Raum Szenario im antiferromagnetischen Bereich des Plots nicht ausgeschlossen werden. Die verschiedenen Verhalten der THE-Isothermen im AFM und PM Bereich deuten auf ein lebendiges Zusammenspiel von Topologie und Magnetismus im Material $EuCd_2As_2$ hin, was ein spannendes Thema für zukünftige

Studien sein kann.

# Contents

# 1 Theory Introduction

In this work, we used different terms to describe each Hall effect contribution seperately. After adding them up again, we must get the whole measured Hall effect. Each of the three terms represent a Hall effect contribution with a different physical origin. Even if the used mathematical description of the different Hall effects are quite easy to use, the theory backing them up is not straight forward. The theory of the ordinary Hall effect, for example, is well explained so that we can derive an equation that connects the relevant quantities with little efforts. But already when we move to the extraordinary Hall effect, the literature has more than one possible explaination that can cause this effect and we have to work with two different phenomenological equations. When we get to the topological Hall effect, quantum mechanics is needed to even understand the basics of this phenomenon. So in this section I want to discuss the relevant theories and sources used in this thesis.

## 1.1 Phenomenon of the Hall Effect

The Hall effect is named after Edvin Hall, who wrote his dissertation 1879 about this phenomenon. The reason why Hall started to study the effect was that he doubted Maxwell's statement, where he described the electric current as a fluid. The effect can be described as follows:
If we look at a current carrying conductor, the term Hall effect describes the phenomenon, that under certain conditions we can measure an electric field orthogonal to the electric field which is causing the current. The conditions that trigger this effect vary from external parameters like magnetic fields to material based properties of the conductor like the magnetization.

## 1.2 Ordinary Hall Effect

When a magnetic field is applied orthogonal to a current carrying conducter, then an electric field can be measured orthogonal to both of them, the magnetic field and the direction of current flow. This transverse electrical field is called Hall field. The phenomenon that a current carrying conductor reacts to a magnetic field with a transverse Hall field, is called the ordinary Hall effect (OHE). To relate the theory with the physical measurement, there are two definitions that have to be introduced: The Hall resistivity $\rho_{xy}$ and the Hall coefficient $R_0$. In our derivation we use a system where the current, powered by the electric field $\mathrm{E_x}$, flows in positive x direction, the magnetic field $\mathbf{B}_z$ acts in positive z direction and the resulting electric Hall-field $\mathrm{E_z}$ appears in positive y direction (see Fig.1).

This effect can be derived starting with the Lorentz force, which is defined as [11]:

$$F = q \cdot (\mathbf{E} + \mathbf{v} \times \mathbf{B}) \tag{1}$$

For describing the motion of electrons in metals under de influence of the Lorenz force, we can use drude's theory [11]. With the three assumptions:

1. $\tau$ is the average time that lies between two scattering events of the moving electrons.
2. When an electron scatters, the momentum p returns to 0. After that it will be accelerated again.
3. The electrons react to the E and B fields the same was as free electrons.

Now we constuct the thermal average $\langle p(t) \rangle$ for a time t + $d$t: We can see that $dt/\tau$ is equivalent to the probability that the electron will scatter. After the scattering process the electron has momentum 0. The complementary probability $(1 - dt/\tau)$ represents all the cases where there is no scattering after $d$t and the momentum will grow from p(t) to p(t) + F$dt$. This results in the formula:

$$\langle \mathbf{p}(\mathrm{t} + dt) \rangle = \left(1 - \frac{dt}{\tau}\right)(\mathbf{p}(t) + \mathbf{F}dt) + \mathbf{0}\frac{dt}{\tau} \tag{2}$$

The last term gives no contribution since it multiplies with the momentum 0. By using the differential quotient $\frac{d\mathbf{p}}{dt} = \frac{\mathbf{p}(\mathrm{t}+dt)-\mathbf{p}(t)}{dt}$ and keeping only linear terms in $dt$ we end up with the expression:

$$\frac{d\mathbf{p}}{dt} = \mathbf{F} - \frac{\mathbf{p}}{\tau} \tag{3}$$

Here we can use Eq. 1 and have:

$$\frac{d\mathbf{p}}{dt} = \mathrm{q} \cdot (\mathbf{E} + \mathbf{v} \times \mathbf{B}) - \frac{\mathbf{p}}{\tau} \tag{4}$$

We can rewright $\mathbf{p}$ as $m\mathbf{v}$, take the last term to the LHS and take the magnetic field $\mathbf{B}$ along the z axis: $\mathbf{B}_z = \mathrm{B} \cdot \mathbf{e_z}$:

$$m\left(\frac{d}{dt} + \frac{1}{\tau}\right)\mathbf{v} = \mathrm{q}(\mathbf{E} + \mathbf{v} \times \mathrm{B} \cdot \mathbf{e_z}) \tag{5}$$

If we split the vectors into their components, we get three seperate equations of motion[4]:

$$\begin{aligned} m\left(\frac{d}{dt} + \frac{1}{\tau}\right)v_x &= \mathrm{q}(\mathrm{E_x} + \mathrm{B}v_y) \\ m\left(\frac{d}{dt} + \frac{1}{\tau}\right)v_y &= \mathrm{q}(\mathrm{E_y} - \mathrm{B}v_x) \\ m\left(\frac{d}{dt} + \frac{1}{\tau}\right)v_z &= \mathrm{qE_z} \end{aligned} \tag{6}$$

We look at the case where the electrical field is static. Thus we can set the time derivatives to

zero. After multiplying equations 6 with $\tau$ and deviding with $m$ we end up with:

$$v_x = \frac{\mathrm{q}\tau}{m}(\mathrm{E_x} + \mathrm{B}v_y) = \frac{\mathrm{q}\tau}{m}\mathrm{E_x} + \omega_c \tau v_y \tag{7}$$

$$v_y = \frac{\mathrm{q}\tau}{m}(\mathrm{E_y} + \mathrm{B}v_x) = \frac{\mathrm{q}\tau}{m}\mathrm{E_y} - \omega_c \tau v_x \tag{8}$$

$$v_z = \frac{q\tau}{m}\mathrm{E_z} \tag{9}$$

Where $\omega_c$ in Eqs. 7 - 9 is the cyclotron frequency defined as $\omega_c = q\mathrm{B}/m$.

Because we think of the current carrying conducter as a rod, the current can not flow out of it, so we have $\delta v_y = 0$. With Eq.7 and Eq.8 we end up with the expression:

$$\mathrm{E_y} = \omega_c \tau \mathrm{E_x} = \frac{q\mathrm{B}\tau}{m}\mathrm{E_x} = -\frac{e\mathrm{B}\tau}{m}\mathrm{E_x} \tag{10}$$

In the last step of Eq.10 the charge q was replaced with the electron charge $-e$. Notice that $e$ is defined positive since the sign is treated seperately! In Eq.10, we can see the direct proportional connection between the current generating electric field $\mathrm{E_x}$ in x direction and the electric Hall field $\mathrm{E_y}$ in y direction.

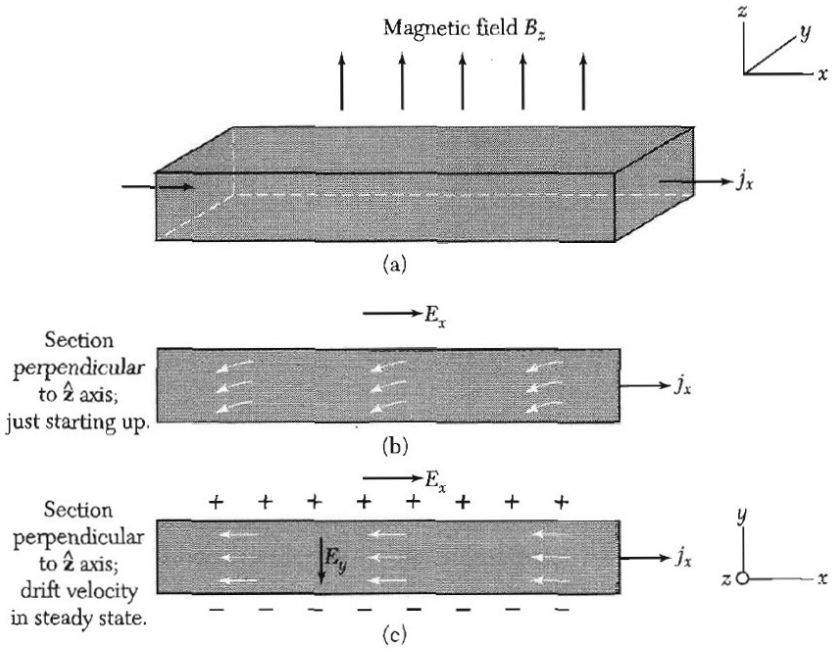


Figure 1: (a): The Orientation of the current carrying conductor, the applied magnetic field and the current density direction is shown. (b) When applying an electric field to generate a current, the Lorentz force pushes the electrons to one side of the conductor. (c) The electron gradient in the conductor leads to a Hall field $E_y$ in y-direction which counter balances the Lorentz force. This leads to a steady state as long as the parameters are kept constant. Image taken from *Introduction to Solid State Physics* by Charles Kittel [4].

The Lorentz force in z direction caused by the B field (Fig. 1a) pushes the electrons to one side of

the rod (Fig.1b). On the other side there are electrons missing for canceling the electric charge so that there is a positive ion excess. This causes a Hall field $\mathrm{E_y}$. The separation continues untill the transverse Lorentz force and the Hall field $\mathrm{E_y}$ cancel each other (Fig.1c). The Hall coefficient is defined as follows:

$$R_0 = \frac{\mathrm{E_y}}{j_x \mathrm{B}} = \frac{\rho^O_{xy}}{\mathrm{B}} \tag{11}$$

In the last step of Eq.11, we used the definition $\rho_{xy} = \frac{\mathrm{E_y}}{j_x}$. Solving Eq.11 for the resistivity we get one of the important equation used in this thesis:

$$\boxed{\rho^O_{xy} = \frac{\mathrm{E_y}}{j_x} = R_0 \mathrm{B} \ \propto R_0 H} \tag{12}$$

In the last step we used the relation $B = \mu_r \mu_0 H$ which is correct under the condition that the current carrying material is isotropic and linear [8]. In the final result, we can see that the ordinary Hall resitivity is proportional to the applied magnetic field B.

## 1.3 Anomalous Hall Effect

The definition we will use in this thesis is that every contribution to the measured overall Hall effect that is not caused by the ordinary Hall effect is ascribed to the anomalous Hall effect. In mathematical form this can be written as:

$$\rho_{xy} = \rho^O_{xy} + \rho^A_{xy} \tag{13}$$

where $\rho^A_{xy}$ is the anomalous Hall effect (AHE), $\rho^O_{xy}$ is the ordinary Hall effect (OHE) and $\rho_{xy}$ is the overall measured Hall effect.

AHE is then further split in two separate contributions:

$$\rho^A_{xy} = \rho^T_{xy} + \rho^E_{xy} \tag{14}$$

where $\rho^E_{xy}$ is the extraordinary Hall effect (EHE) and the $\rho^T_{xy}$ is the topological Hall effect (THE).

### 1.3.1 Extraordinary Hall Effect

This effect doesn't rely on a magnetic field and can therefore also occur in a magnetic field free environment. It is commonly described by the phenomenological equation [2]:

$$\rho^E_{xy} = \mu_0 R_e M \tag{15}$$

where $\rho_{xy}^E$ is the extraordinary Hall resistivity, $M$ the magnetization, $\mu_0$ the vacuum permeability and $R_e$ the extraordinary Hall coefficient. It took more than sixty years to clear up the origin of the effect theoretically [7].

$R_e$ is $\propto \rho_{xx}^n$ where $n$ does depend on the predominant scattering mechanism that occurs in the material: for skew scattering n = 1 and for the intrinsic deflection n = 2 [2]. $\rho_{xx}$ is the longitudinal resistivity. So we can rewrigt Eq.15 into two equations:

skew scattring: intrinsic deflection:

$$\boxed{\rho_{xy}^E = \mu_0 \rho_{xx} M} \quad (16) \qquad \boxed{\rho_{xy}^E = \mu_0 \rho_{xx}^2 M} \quad (17)$$

Skew scattering is a phenomenon that occurs because of impurities in the material [6] and introduces different peferential scattering directions for spin-up and spin-down particles [7]. Since there are not equal many spin-up as spin-down electrons in a ferromagnet, the separation of spin states will lead to a extraordinary Hall effect [7].

The intrinsic deflection is a phenomenon which occurs when an electric field acts on the electrons. The electric field produces different velocity vectors perpendicular to the motion of travel which don't sum up to zero. This effect is called interband coherence and leads to a nonsymmetrical split which gives rise do a extraordinary Hall effect. [5]

In the two equations 16 and 17 we can see that the extraordinary Hall resistivity $\rho_{xy}^E$ is either proportional to $\rho_{xx} M$ (skew) or to $\rho_{xx}^2 M$ (intrinsic).

### Remark

For completition I want to mention that if both phenomenas occur at the same time, Eqs. 16 and 17 can be combined to one equation [2]:

$$R_e^s = a\rho_{xx} + b\rho_{xx} \quad (18)$$

where a and b are coefficients corresponding to the skew scattering and side jump, respectively. [2] In our case we calculated two separate versions assuming that only one of the phenomenas was causing the extraordinary Hall effect. As we shall see later in the results, both versions are almost identical.

### 1.3.2 Topological Hall Effect

Not long ago it was found that in certain types of frustrated ferromagnetic systems with non-coplanar magnetic moments the coefficient $R_e$ did not follow the expectations from the extraordinary Hall effect theory [7]. In order to explain this new effect, a new mechanism was proposed called topological Hall effect [7]. The topological Hall effect can have different types of origins: In one scenario the THE is caused by the real space picture linked to to the topology of the magnetization texture of the material. In another scenario the THE is caused by a reciprocal band structure picture linked to a phenomenon called Weyl nodes, also called momentum space scenario. In what follows, both cases are presented with more detail.

#### Topological Hall Effect of Real Space Scenario

The real space scenario is when the interaction of an electron spin with the non coplanar topology of a material structure leads to a Berry phase. This phase can also be interpreted as being produced by a spinless electron moving in a spatially varying magnetic field. For every angle subtended in a cell structure, the amount of magnetic flux can be calculated to achieve the same reaction of an electron moving past the same cell (see Fig. 2). Sumarized it can be said that the Hamiltonian of an electron moving in a magnetization texture can be mapped onto a Hamiltonian of a spinless electron moving in an inhomogeneous magnetic flux distribution [7]. Because of this equivalence, the topological Hall effect can be understood.

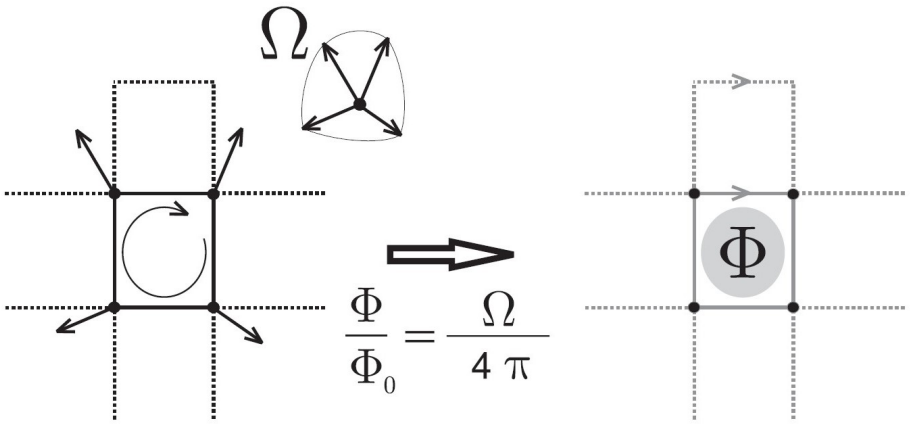


Figure 2: If an electron is assumed to follow a closed trajectory around a lattice cell as seen left, the electron will pick up a Bery phase if the texture is noncoplanar [7]. Since a Berry phase can also be produced by a magnetic flux piercing through the same cell (as seen right), an equivalence relation can be formed. Image taken from *Electronic transport in mesoscopic systems* by Georgo Metalidis [7].

### Topological Hall Effect of Momentum Space Scenario

The momentum space scenario is based on Weyl nodes, which act as a source and a sink of Berry curvature [12]. In this scenario the topological Hall effect is proportional to the Brillouin-zone integration of the Berry curvature [1]. Since the Berry curvature is related to the Berry phase via a closed-path integration we can make the same equivalence relation and come to the conclusion, that the reaction of an electron to a pseudo-field attributed to a Weyl node can't be distinguished from the reaction of an electron reacting to a real external applied magnetic field. [3]. Therefore the Weyl nodes as an origin of the topological Hall effect can be understood.

## 1.4 Paramagnetism, Antiferromagnetism and Ferromagnetism

All informations in this subchapter 1.4 are based on *Elektrodynamics* by Wolfgang Nolting [9], unless otherwise stated.

Paramagnetism (PM) is the phase in which the magnetic moments of a material can align with an outer magnetic field so that the field measured inside the material is stronger than on the outside. If no magnetic field is applied, no magnetic field can be measured from the material.

Antiferromagnetism (AFM) is the phase in which the magnetic moments of a material do cancel each other so that no net magntic field can be measured wether there is a magnetic field acting from the outside or not.

The temperature that separates paramagnetism and Antiferromagnetism is called the Néel temperature $T_N$. Below $T_N$ the material is AFM and above $T_N$ the material is PM. For $EuCd_2As_2$ $T_N \approx 9.5K$ [10].

Ferromagnetism (FM) is the phase when the magnetic moments of a material align with the magnetic field and preserve a remanent magnetization when the external magnetic field is turned off. This phenomenon leads to a permanent magnet. The connection of the remanent magnetization and the applied magnetic field can be described with a hysteresis.

The temperature that separates ferromagnetism and paramagnetism is called the Curie temperature $T_C$. Below $T_C$ the material is FM and above $T_C$ the material is PM.

The different reactions of the magnetic moments to a magnetic field are shown in Fig.3:

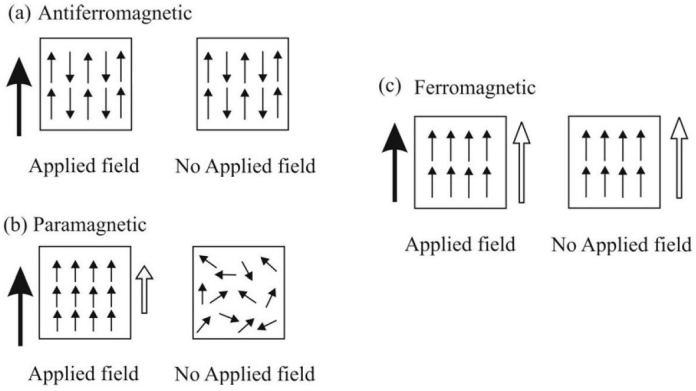


Figure 3: The black arrow represents the applied magnetic field while the white arrow represents the response field of the material. (a) The antiferromagnetic phase doesn't reaction to an external magnetic field. (b) In the paramagnetic phase the material reacts mildly (white arrow) to the external magnetic field and loses its internal magnetic moment alignment when the magnetic field is turned off. (c) In the ferromagnetic phase the material react strongly to an external magnetic field and keeps a remanent magnetisation after turning off the external magnetic field. The material is then called a permanent magnet.

# 2 Methods and Results

In this section, I will discuss the steps and methods used to process the given data of $EuCd_2As_2$ and present the obtained results. The program that was used for processing is called Origin Lab. The fitting of the isotherms was done with the built in linear fit option of Origin Lab.

## 2.1 Methods and Data Acquired

The data was obtained by using commercial Quantum Design Magnetic and Physical Property Measurement Systems (MPMS and PPMS). For the resistivity experiments a Hall-bar electrical contact geometry was created. Good electrical contacts ($\sim$1 $\Omega$) were established using DuPont 6838 silver paste cured at 500 °C for 10 min and subsequent application of short high voltage pulses. For the thermoelectric transport a home-built insert for the PPMS was used. The temperature gradient in the sample was held at $\approx$3% of the sample temperature and was measured with Cernox thermometers, while the voltage was measured using nanovoltmeters. For all measurements magnetic fields were applied along the easy-c-axis.

For this thesis, the following measured data was used:

- Magnetic field strength H [T]
- Temperature T [K]
- Overall Hall resistivity$\rho_{xy}$ [$\Omega$ m]
- Resistivity $\rho_{xx}$ [$\Omega$ m]
- Magnetization M [$\frac{A}{m}$]

16 measurements were done at different temperatures. During a measurement, the temperature was held constant. The isotherms obtained were taken at the temperatures: 2K, 4K, 5K, 6K, 8K, 10K, 12K, 15K, 18K 20K, 25K, 30K, 40K, 60K, 80K, 100K.

## 2.2 Raw Data of $EuCd_2As_2$ Measurement

In Fig.4 and Fig.5 the temperature- and magnetic field dependence of Hall resistivity $\rho_{xy}$, longitudinal resistivity $\rho_{xx}$ and the magnetization $M$ of $EuCd_2As_2$ are shown:

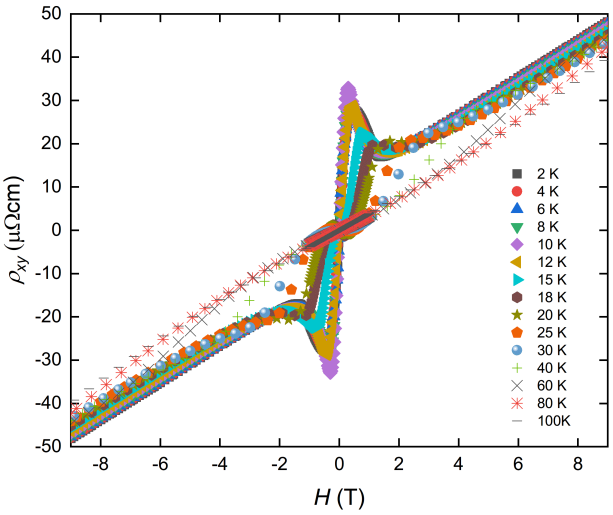


Figure 4: Raw Hall resistivity $\rho_{xy}$ of $EuCd_2As_2$ at temperatures between 2-100K plotted against the magnetic field strength H. Every isotherm consists of three compounds, OHE, EHE and THE, added together. The separation and interpretation of these components is the goal of this thesis.

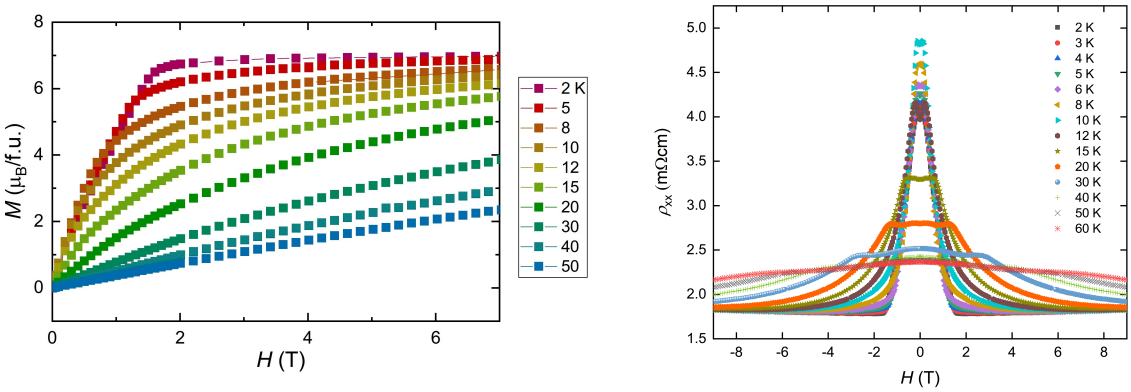


Figure 5: On the left hand side: Raw magnetization $M$ of $EuCd_2As_2$ at different temperatures plotted against the magnetic field strength H. On the rigth hand side: Raw linear resistivity $\rho_{xx}$ of $EuCd_2As_2$ at temperatures between 2-60K plotted against the magnetic field strength H. Both plots are later used to obtain the EHE of $EuCd_2As_2$.

According to Eq.13 and Eq.14 from the introduction section, the isotherms of Fig.4 can be split into three compounds $\rho_{xy} = \rho_{xy}^O + \rho_{xy}^E + \rho_{xy}^T$. In order to separate the contributions, the linear

fitting of the raw data $\rho_{xy}$ is shown in section 2.3. Then, in section 2.4, the linear fitting of the EHE is shown, which also consists of the raw data $\rho_{xx}$ and $M$. These two fits then will lead us to the final step of extracting the topological Hall effect of $EuCd_2As_2$ in section 2.5. In section 2.6 the final results can be presented in two 3D plots.

## 2.3 Extracting Slope and Intersect of measured $\rho_{xy}$

For beeing able to use the linear fitting method, we first have to find the linear part of $\rho_{xy}$. The following facts are known:

- The ordinary Hall effect is linear everywhere.
- The extraordinary Hall effect is non-linear in the low field part but from a certain field strength on in our case is almost linear (and also nearly constant) in high field and therefore will be linearly approximated in this part.
- The topological Hall effect is non-linear in the low field part and gets negligibly small from a certain field strength on in the high field part.

For being able to make a reasonable linear fit to $\rho_{xy}$, all contributions have to be linear in the fitted region. The component who gets linear last (EHE or THE), defines the magnetic field strength, which distinguishes the low and high field part of $\rho_{xy}$. In summary this means, that the deviation from linear of an isotherm in the measured Hall resistivity $\rho_{xy}$ defines a field scale that separates the low and high field part.

After defining the high field part of the isotherms, the fit of the overall Hall resistivity data $\rho_{xy}$ gives us the slope a and the intersect b:

$$\text{high-field part of } \rho_{xy} = a \cdot H + b \tag{19}$$

The vertical intersect b is not used in this section, but will get important later on in section 2.5 and is therefore also extracted. The procedure of defining the high field part of the isotherm, followed by a linear fit to extract the slope a and the intersect b was done for every isotherm measured. As an example, the segmentation of the data can be seen in Fig.6 for the cases 2K (L.H.S.) and 40K (R.H.S). In this section, both slopes of EHE and THE are treated as negligible in the high field part. This is a good first approximation and allows us to set the extracted slope equal to the ordinary Hall coefficient: $a = R_0$. After subtracting the first aproximation of the ordinary Hall effect ($R_0 H$) from the overall measured Hall resistivity $\rho_{xy}$, we are left with the red line (Fig.6), representing the anomalous Hall effect (EHE + THE).

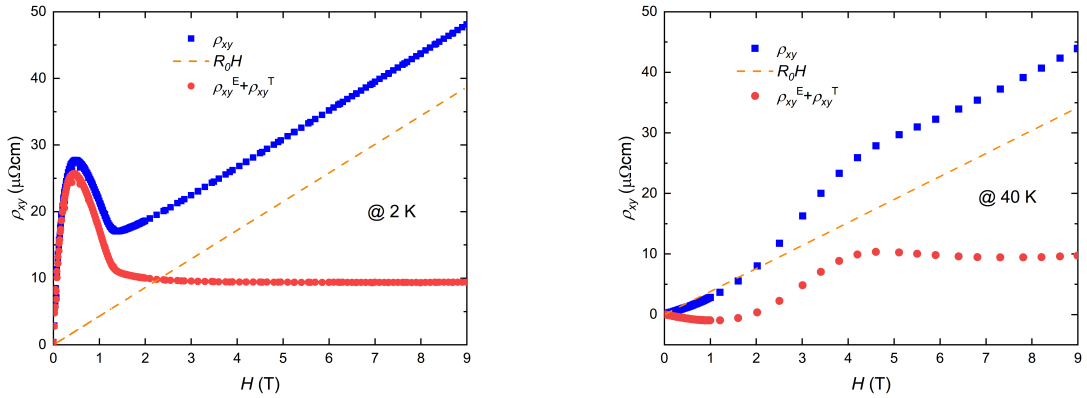


Figure 6: Data of $EuCd_2As_2$ after subtracting the extracted first approximation OHE at 2K (L.H.S.) and 40K (R.H.S).

## 2.4 Extracting Slope and Intersection of measured $\rho_{xy}^E$

In section 2.3, we treated the slope of the EHE as beeing zero in the high field part. In the next two sections we will see that this was indeed a good approximation. However, for extracting the most accurate THE, the fit of the data of $\rho_{xy}^E$ is crucial and will be needed in the next section to evaluate the exact contribution of the EHE in the measured Hall resistivity $\rho_{xy}$.
The extraordinary Hall resitivity was constructed following the Eq. 16: $\rho_{xy}^E = \mu_0 \rho_{xx} M$ for skew scattering and Eq.17: $\rho_{xy}^E = \mu_0 \rho_{xx}^2 M$ for intrinsic deflection from our theory section. This was done by multiplying the measured data $\rho_{xx}$ from (R.H.S. in Fig.5) with the measured data $M$ from (L.H.S. in Fig.5). Since only the proportionality of $\rho_{xy}^E$ is used later on, we could ignore the factor $\mu_0$.
The fitting process was the same as in section 2.3: For beeing able to use the linear fitting method, we again had to find the linear high field part of the measured extraordinary Hall resistivity $\rho_{xy}^E$, which was done by using the deviation from linear of an isotherm to define the field scale that separates the low and high field part. The resulting fit gave us the Slope c and Intersect d as seen in Eq.20:

$$\text{high-field part of } \rho_{xy}^E = c \cdot H + d \tag{20}$$

Slope c and intersect d will help to scale the EHE for subtracting the correct sized anomalous Hall effect from the measured Hall resistivity $\rho_{xy}$. But for doing this, a new scaling factor has to be introduced: $S_H$.

## 2.5 Combinating Fits with Parameters $R_0$ and $S_H$

In this chapter, the two fits done in section 2.3 and 2.4 allow us to establish an accurate formula that scale the OHE and EHE correctly, leading us to the correct extraction of the topological Hall effect.
As already mentioned, compared to the high-field part of the topological hall effect (which is constant 0), the high-field part of the EHE has a small slope c. This means that the equivalence $a = R_0$ has to be corrected. The corrected ordinary Hall coefficient will be written as $R_0'$. For finding the correct $R_0'$, our separation process of the measured $\rho_{xy}$ will now be written down in terms of the fitting processes, stated in Eq. 19 and Eq. 20:

$$\rho_{xy} \quad = \quad \rho_{xy}^{O} \quad + \quad \rho_{xy}^{E} \quad + \quad \rho_{xy}^{T} \tag{21}$$

$$a \cdot H + b \;=\; R_0' \cdot H \;+\; S_H(c \cdot H + d) + \;\rho_{xy}^{T} \tag{22}$$

Where in Eq.22 the LHS of the equation is the fit of the measured Hall resistivity $\rho_{xy}$ and on the RHS of the equation (from left to right) is the ordinary Hall effect, the fit of the extraordinary Hall effect multiplyed with a scaling factor $S_H$ and the topological Hall effect $\rho_{xy}^{T}$. $S_H$ is an additional parameter that makes sure that the intersect d of the EHE fit deletes the intersect b from the overall Hall effect fit. This is a concequence of the fact that the EHE is the only of the three contributions who has a constant offset in high field.
After realizing that $\rho_{xy}^{T}$ is zero in high-field and rearranging Eq.22 we get:

$$0 = (R_0' - a + S_H \cdot c)H + S_H \cdot d - b \tag{23}$$

For the R.H.S. to be zero in Eq. 23 the two terms $(R_0' - a + S_H \cdot c)$ and $(S_H \cdot d - b)$ have to be zero. Therefore we have the final two equation which give us the correlation between the fitting parameters a,b,c and d, and the scaling factors $R_0'$ and $S_H$ :

$$\boxed{S_H = \frac{b}{d}} \tag{24}$$

$$\boxed{R_0' = a - \frac{b}{d} \cdot c} \tag{25}$$

In Eq.25 we can see the correction term $-\frac{b}{d} \cdot c$ of the ordinary Hall coefficient.
Applying the results to the data, we first correct the OHE and subtract it from the measured resistivity $\rho_{xy}$ to get the corrected anomalous Hall effect. Then we scale the extraordinary Hall resistivity with the factor $S_H$ and subtract it from the anamolous Hall resistivity to get the extracted topological Hall resistivity. As an example, the cases 2K (L.H.S) and 40K (R.H.S.) are shown in Fig. 7, where we can see the corrected contribution of the OHE (orange dotted

line), the $S_H$ scaled EHE and our final extraction of the topological Hall effect at 2K and 40K (red dotted line). It can also be seen how small the correction to $R_0$ is since EHE is almost constant in high-field which leads to a small slope c in the fit.

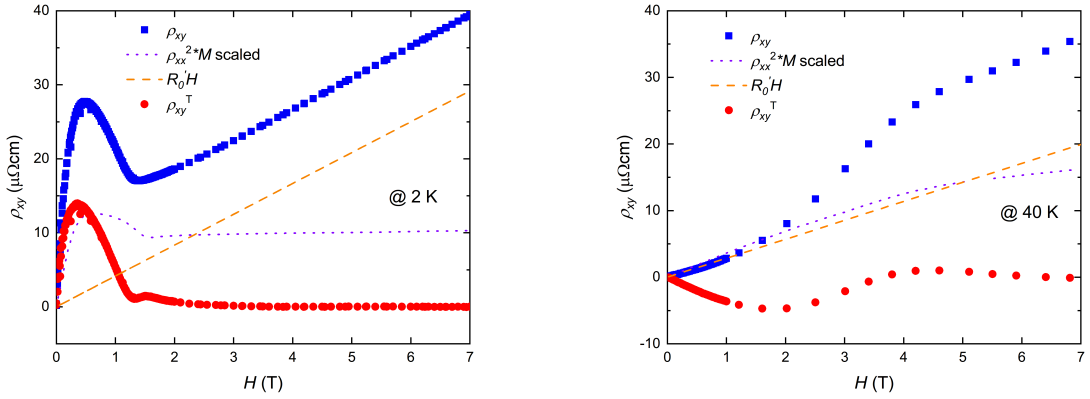


Figure 7: Raw Hall resistivity $\rho_{xy}$ (blue isotherm) at 2K (L.H.S.) and 40K (R.H.S.) measured on $EuCd_2As_2$ split into their contributions: corrected OHE (orange curve), EHE in intrinsic deflection scenario (purple curve) and THE (red curve).

## 2.6 Diagram of Topological Hall Effect Depending on Temperature and Magnetic Field

Repeating the procedure shown above for every temperature measured, we can summarize the fndings in 3-D colour plots. Since the extraordinary Hall effect has two different outcomes for each temperature depending on what scattering mechanism is present in the material, we end up with two plots seen in Fig. 8:

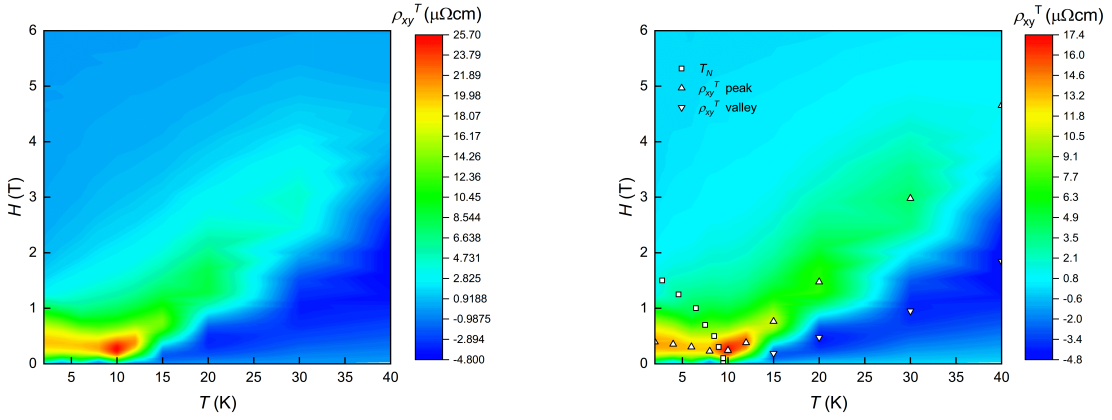


Figure 8: On the L.H.S.: Summarized plot for extracted THE for skew scattering mechanism. On the R.H.S.: Summarized plot for extracted THE for intrinsic deflection. Here also $T_N$ = Neel temperature, local maxima and local minima are marked.

# 3 Discussion, Conclusion and Outlook

It can be clearly seen that the two 3-D colour plots are very similar regardless of which scattering mechanism scenario was used for the EHE. Both scenarios have their maximas at ca. 10 K and ca. 0.3T. In the case of the skew mechanism the tolopogical Hall resistivity ranges from -4.8 to 25.7 $\mu\Omega cm$ and therefore is a bit lower than the resistivity range of the intrinsic mechanism which goes from -4.8 to 17.4 $\mu\Omega cm$.

There are 4 observations that can be made from the 3D colour plot and suggest that the mechanisms of the THE in the AFM and the PM state are different [13].:

- The local maxima of the resistivity are highest near the Neel temperature.
- The minimal magnetic field strength at which an isotherm reaches it's local maximum is also found near the Neel temperature.
- The width of the local maxima is smallest around the Neel temperature.
- Negative values of the THE resistivity are only found in the PM state.

First lets discuss the PM state ($T > T_N$): Since in other studies there was solid evidence found for Weyl points in the material $EuCd_2As_2$ that are lying in the vicinity of the Fermi level already at zero field, the Weyl points are a good candidate for producing the THE in the PM state and could also explain both signs of the THE in the PM phase [13].
In the AFM state ($T < T_N$) of $EuCd_2As_2$, where the magnetic moments are coupled along the c axis, the spins, aligned by a finite H field along the c axis, would create Weyl points which then give rise to a THE [13]. So the Weyl points are also the most probable candidates to generate the measured THE in the AFM state. But because the AFM part of $EuCd_2As_2$(R.H.S. of Fig. 8) has also some similarity to systems that have real-space induced THE we can't exclude a real-space contribution to the THE in the AFM state [13].

In conclusion we were able to extract the topological Hall effect of the material $EuCd_2As_2$ at different temperatures and magnetic fields. The observed THE in the PM state represents a rare case of topological transverse transport beyond the ordinary and conventional anomalous contribution in the absence of long-range magnetic order [13]. From our results we claim the Weyl points to be responsible for the topological Hall effect in both AFM and PM state. Since in the AFM state a real-space scenario contribution to the THE can't be excluded, further measurements would be required to prove or falsify this possibility. Since the spin configuration affects the electronic band structure significantly, the distinct mechanisms in the AFM and PM state suggest a vivid interplay of magnetism and topology in the material $EuCd_2As_2$ [13].

The decomposition and discussion of the Hall resistivity, measured in $EuCd_2As_2$, was able to make assumtions on the origins of the extracted THE that are also covered by other available studies. It further generated new data that can now be included in theoretical studies on $EuCd_2As_2$. The analysis of the data also poses questions which incentivize to do additional research for getting better insights into the interplay of magnetism and topology in $EuCd_2As_2$. With further studies we then could verify or falsify the real-space induced topological Hall effect in the AFM spectrum of $EuCd_2As_2$.

# Acknowledgement

I want to thank Prof. Johan Chang of the University of Zürich for giving me the opportunity of doing this bachelor thesis in his research group and introducing me to the fascinating research work done by him and his group. His patience and support lead me to the dedication for this project. He also provided me with additional material for studying the Hall effect.
I also want to thank Yang Xu for supervising me during the whole bachelor project, helping me to understand the theoretical part of the experiment and often supplying me with inevitable advices during the writing process.
Further thanks go to Catherine Witteveen and Stefanie Jucker for helping me with the layout of this thesis and general latex-related questions.

# References


[1] Hua Chen, Qian Niu, and Allan H MacDonald. "Anomalous Hall effect arising from non-collinear antiferromagnetism". In: *Physical review letters* 112.1 (2014), p. 017205.

[2] A Gerber et al. "Extraordinary Hall effect in magnetic films". In: *Journal of magnetism and magnetic materials* 242 (2002), pp. 90–97.

[3] Roni Ilan, Adolfo G Grushin, and Dmitry I Pikulin. "Pseudo-electromagnetic fields in 3D topological semimetals". In: *Nature Reviews Physics* (2019), pp. 1–13.

[4] Charles Kittel. *Introduction to Solid State Physics*. Vol. 8. John Wiley & Sons, 2005, pp. 147–156.

[5] Xufeng Kou, Yabin Fan, and Kang L Wang. "Review of quantum Hall trio". In: *Journal of Physics and Chemistry of Solids* 128 (2019), pp. 2–23.

[6] A. Macdonald and Jairo Sinova. *Theory of spin-orbit effcts in semiconductors*. Jan. 2014, pp. 16–17.

[7] Georgo Metalidis. "Electronic transport in mesoscopic systems". In: (2007), pp. 71–80.

[8] Wolfgang Nolting. *Elektrodynamik*. Springer, 2007, pp. 205–206.

[9] Wolfgang Nolting. *Elektrodynamik*. Springer, 2007, pp. 206–211.

[10] Inga Schellenberg et al. "A 121Sb and 151Eu Mössbauer spectroscopic investigation of EuCd2X2 (X= P, As, Sb) and YbCd2Sb2". In: *Zeitschrift für anorganische und allgemeine Chemie* 637.12 (2011), pp. 1863–1870.

[11] Steven H Simon. *The Oxford solid state basics*. OUP Oxford, 2013, pp. 19–21.

[12] J-R Soh et al. "Ideal Weyl semimetal induced by magnetic exchange". In: *Physical Review B* 100.20 (2019), p. 201102.

[13] J Chang Y. XU L. Das and T. Shang. "Topological transverse transport in the presence and absence of magnetic order in $EuCd_2As_2$". In: *submitted for publication* (2020).